Supporting information for

Optical Nature and Binding Energetics of Fluorescent Fluoride Sensor Bis(bora)calix[4]arene and Design Strategies of its Homologues

Jaehyeok Jin[1], Ji Young Park[2], and Yoon Sup Lee[3]

Department of Chemistry, Korea Advanced Institute of Science and Technology (KAIST), Yuseong-gu, Daejeon 34141, Korea

E-mail: yslee@kaist.edu

[1] Present address: Department of Chemistry, The University of Chicago, 5735 South Ellis Avenue, Chicago, Illinois 60637, United States

[2] Present address: Center for Catalytic Hydrocarbon Functionalization, Institute for Basic Science (IBS), Daejeon 34141, Korea

[3] To whom correspondence should be addressed. Tel: +82-42-350-2821; Fax: +82-42-350-2810

S1. Calculated ^{1}H NMR shifts of 1

Calculated ^{1}H NMR chemical shifts (a left column in Table S1) and experimental data[1] (a right column in Table S1) of bis(bora)calix[4]arene, or **1**, are listed in Table S1. These chemical shifts agree with the experimental data to the same degree as other previously reported NMR shift calculations of calixarene derivatives.[2,3]

Table S1. The ^{1}H NMR chemical shifts of bis(bora)calix[4]arene using MPW91PW91/6-31G(d,p) (unit: ppm)

Chemical shift (Degeneracy)		*Cal.*	*Exp.*[1]
Cal.	*Exp.*[1]	7.53 (2H)	6.88 (4H)
8.57 (2H)	7.68 (4H)	7.34 (2H)	
8.50 (2H)		5.49 (2H)	5.01 (2H)
8.11 (2H)	7.22 (4H)	4.23 (2H)	3.89 (2H)
7.89 (2H)		3.56 (2H)	3.47 (2H)
7.62 (2H)	7.03 (2H)	3.37 (2H)	3.36 (2H)
7.57 ~ 7.56 (4H)	6.93 (4H)	1.94 ~ 1.18 (36H)	0.82 (36H)

S2. Vibrational analysis of 1 and F- binding complexes

Vibrational analysis gives two important information about **1** and F^- binding complexes **1-F**: the ground state geometry of the molecules and the vibrational modes that correspond to the structural differences among **1**, *endo*-**1-F**, and *exo*-**1-F**.

Vibrational frequencies are calculated by employing *numerical* command in Gaussian 09 with the ONIOM(B3LYP/6-31+G(d):B3LYP/3-21G) level of theory. Overall vibrations are transformed to IR spectra after calculating the vibrational modes. Figure S1-(a), (b), and (c) show the IR spectra of the **1**, *endo*-**1-F**, and *exo*-**1-F** cases, respectively.

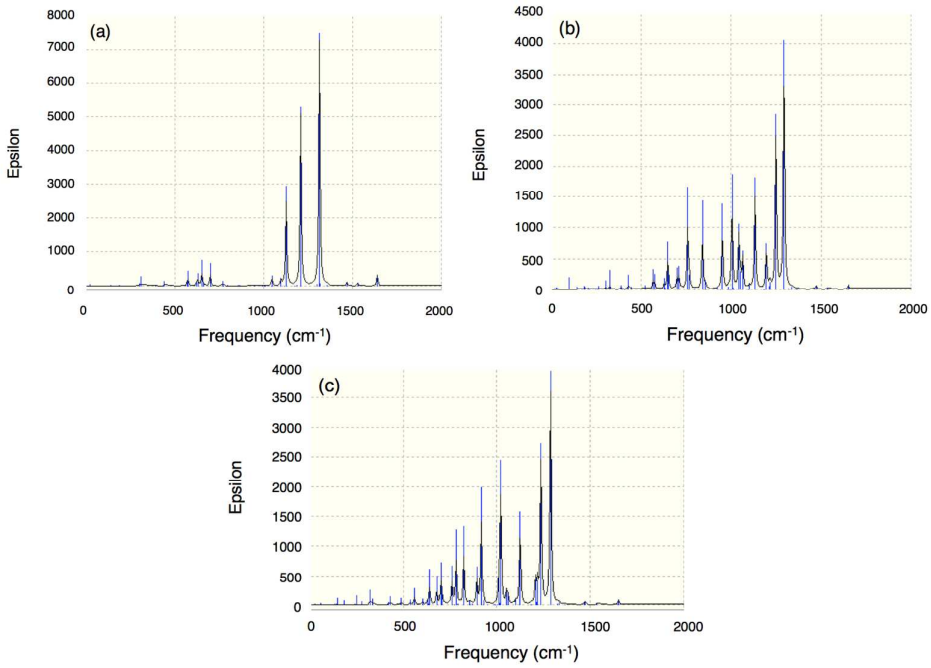

Figure S1. Calculated IR spectra of bis(bora)calix[4]arene and its binding complexes with F^- using ONIOM(B3LYP/6-31+G(d):B3LYP/3-21G) (a) 1 (b) *endo*-1-F (c) *exo*-1-F

The optimized structures have no imaginary frequencies, which indicates the optimized structures of **1** and **1-F** are the true minima on the ground state energy surface. To understand the major changes involved with vibrations while binding with fluoride, we compare the vibrational modes between *endo*-**1-F** and *exo*-**1-F** in the frequency domain from Figure S1.

Firstly, the epsilon values of the binding complexes are half of that of **1**. Although the general profile of the IR spectra remains similar for both binding complexes, some changes appear in the low frequency region and the 500-1200 cm^{-1} region. To further examine these changes, a comparison among the specific vibrations corresponding to the calculated peaks in these regions is conducted, as described below.

In the low frequency region, most of the vibrations are composed of displacements from the two wall benzenes (see Figure S4). There are two specific frequencies that correspond to the symmetrical displacement of the two wall benzenes in **1**: moving in the same direction at 20 cm^{-1} and moving in the opposite direction toward the outer side at 40

cm^{-1}.

However, for binding complexes, these patterns have slightly changed with respect to the *endo* or *exo*-binding mode. For *endo*-**1-F**, a similar trend is observed, but decoupled motions originated by the fluoride are also observed. In detail, the vibrational mode in the same direction is observed at 22 cm^{-1} and the fluoride anion linked to the benzene moiety vibrates together. This additional vibration can affect the reduced mass of the vibrating molecule, resulting in the increased frequency. For *exo*-**1-F**, the vibration toward the outer side is hindered by the *exo*-bound fluoride anion, hence the calculated vibrations show the mixed motion of the inner space stretching in opposite/same directions. In the 200-300 cm^{-1} region, more complicated changes are observed from binding with the fluoride anion. Especially, a large displacement of the fluoride anion is observed at 265 cm^{-1} with wagging motion of the one benzene molecule in the lower rim. However, in the neutral case **1**, this vibration is attributed to the in-plane vibration pattern of the two benzene walls at 252 cm^{-1}. Therefore, in this case, the fluoride anion located between the two benzene rings breaks the symmetry of the motion, resulting in a decoupled motion of each benzene.

At 298cm^{-1}, **1** shows out-of-plane vibrations of the two oxygen-boron moieties with nearly identical intensities. However, *endo*-**1-F** shows asymmetric vibrations of those moieties in a slightly high frequency region at 305 cm^{-1}. In this case, one oxygen-boron pair closest to the fluoride anion tends to move slowly compared to the neutral case because of the presence of the fluoride anion. Interestingly, this pattern is not observed in *exo*-**1-F**, which can be interpreted as a result of the blocking effect of the side-binding fluoride on oxygen-boron stretching. A similar vibrational pattern in the opposite direction is observed at 307 cm^{-1}. Although this pattern is not observed in *exo*-**1-F**, *endo*-**1-F** shows a large displacement of the fluoride at 328 cm^{-1}. This can be also understood as the blocking effect of the fluoride on the certain configurations of vibrations.

Some vibrations in the 820-840 cm^{-1} region contain weak vibrational modes of the fluoride, but these vibrations are considered as reactions from a large displacement of the boron atom. After 900 cm^{-1}, no vibration motion of the fluoride is observed.

In conclusion, the vibration analysis shows the ground state geometries and the structural characteristics of **1**, *endo*-**1-F**, and *exo*-**1-F**.

S3. Optimized geometries of various sensor motifs

S3.1. Optimized geometries of **1-X** (X: Cl-, Br-)

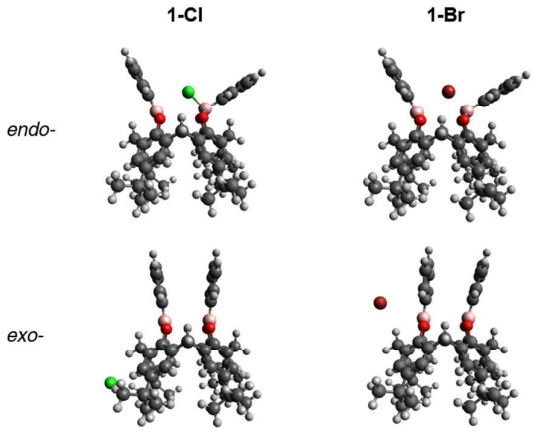

Figure S2. Optimized structures of 1-Cl and 1-Br complexes with both the *endo*- and ***exo*- manners using ONIOM(B3LYP/6-31+G(d):B3LYP/3-21G) in the chloroform solution**

It is worth denoting that *exo*-**1-Cl** (the chloride binding complex of **1-Cl** via the *exo*-mode) is not regarded as an effective binding because it binds to the upper-rim part of **1-Cl**.

S3.2. Optimized geometries of *endo*-**XY-1F** and *exo*-**XY-1F** (**X, Y**: B, P, N, and Al)

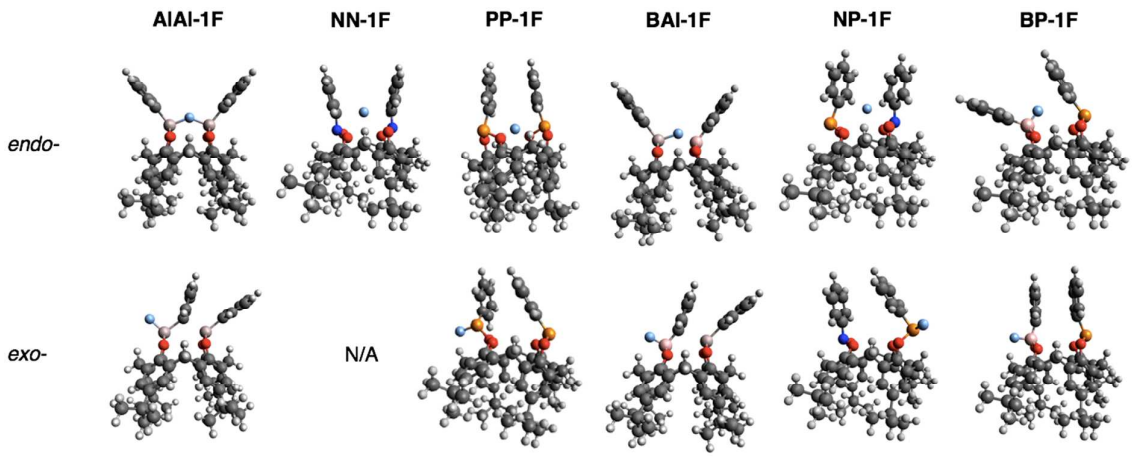

Figure S3. Optimized structures of *endo*-XY-1F and *exo*-XY-1F using ONIOM(B3LYP/6-31+G(d):B3LYP/3-21G) in the gas phase

S4. Fragment separation by Mulliken population in the frontier molecular orbital composition

In order to perform the frontier molecular orbital analysis, we decompose **1** into four fragments: wall benzenes (green), boron atoms (yellow), oxygen atoms (blue), and the main 16-membered ring (red). The fragment decomposition of **1** gives an insight in terms of the nature of transitions at the electronic level.[4] A detailed illustration is shown in Figure S4.

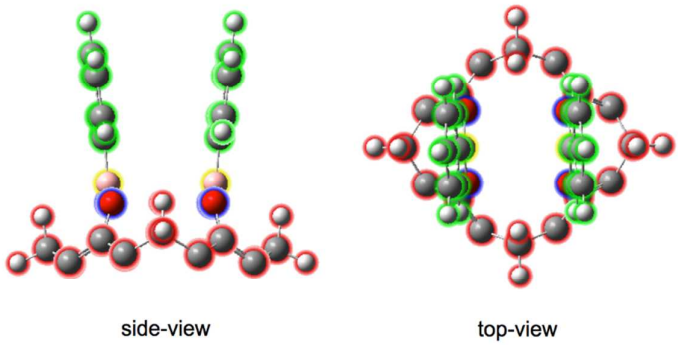

Figure S4. Mulliken fragments of 1 in the frontier MO decomposition

(green: wall benzenes, yellow: boron atoms, blue: oxygen atoms, red: main ring)

S5. Additional TD-DFT calculation in the first excited state

To validate the optimized structure in the S1 excited state, the bond lengths and angles of **1** in the excited state are calculated and compared with the ground state values of the molecule (see Table S2).

Table S2. Calculated geometrical properties of bis(bora)calix[4]arene in the ground and first excited states

(a) Bond lengths

Bond length (Å)	B50-O45	B50-O47	O47-C24	O45-C14	C12-C9	C14-C12	B50-C51
Ground state	1.400	1.399	1.378	1.376	1.528	1.400	1.547
Excited state	1.404	1.412	1.402	1.399	1.528	1.417	1.554
δ (difference)	0.004	0.013	0.024	0.023	0.000	0.017	0.007

(b) Bond angles

Bond angle (°)	∠O45-B50-O47	∠O46-B49-O48
Ground state	121.87	121.87
Excited state	125.86	112.14
δ (difference)	3.99	9.73

Also, the root mean square (RMS) value of overall bond distances is 1.38 Å in the ground state and 1.40 Å in the first excited state, indicating that the general structure remains similar. Figure S5 shows the TD-DFT spectra of **1** in the ground and excited states.

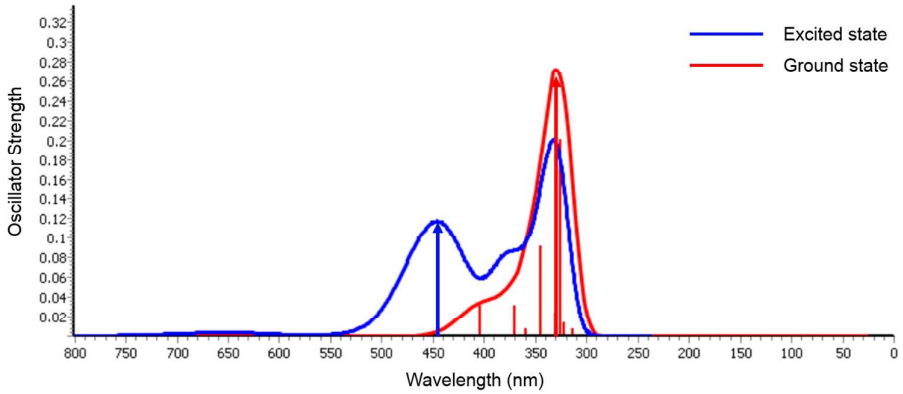

Figure S5. Calculated TD-DFT spectra of 1 in the ground and excited states with denoting important transition peaks as arrows using PBE1W/6-311G(d)

Interestingly, both the ground and excited states spectra have a peak near 320 nm, but they show different patterns in the longer wavelength region near 450 nm. To elucidate the difference in this region, we assess the MO energy level and depict the MO diagrams of **1** in the ground and excited states (see Figure S6).

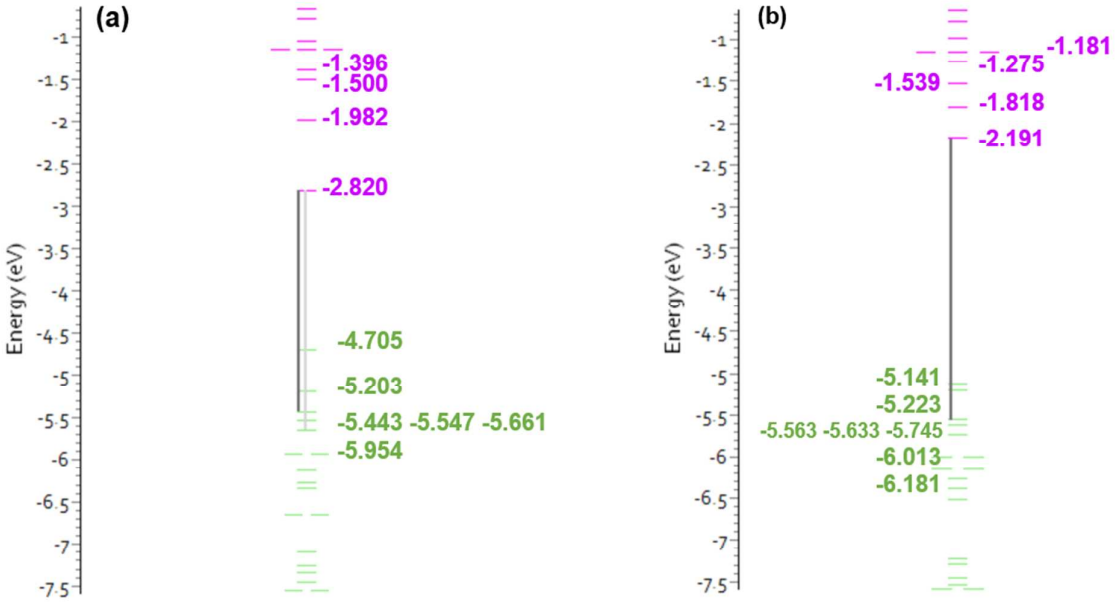

Figure S6. MO diagrams of bis(bora)calix[4]arene in the first excited and ground states with denoting energy values (eV) using PBE1W/6-311G(d):
(a) MO diagram in the excited state. (b) MO diagram in the ground state.

The neutral molecule, **1**, is composed of 220 filled orbitals. Thus the HOMO is located at the 220th MO and the LUMO at the 221th MO. A comparison of Figure S6-(a) with (b) shows that the ground and excited states have similar orders of MO. When **1** is excited to the singlet state, the HOMO energy slightly increases and the LUMO energy slightly decreases, which result in a shift to a longer wavelength region (thus lower energy). This shift to a longer wavelength region is also consistent with the pattern from the simulated spectra. In Figure S5, the strong peak at 330 nm in the ground state, which is marked by a red arrow, originates from the transition of MO 218 to MO 221. However, this transition is shifted to 450 nm in the excited state, which is a mixed transition from 216 to 221 and 218 to 221 (marked by a blue arrow).

To check the electron density in the lower rim, the LUMO and LUMO+1 (221st MO and 222nd MO) of **1,** and the HOMO and HOMO-4 (225th MO and 221st MO) of *endo*-**1-F** complex are depicted in Figure S7.

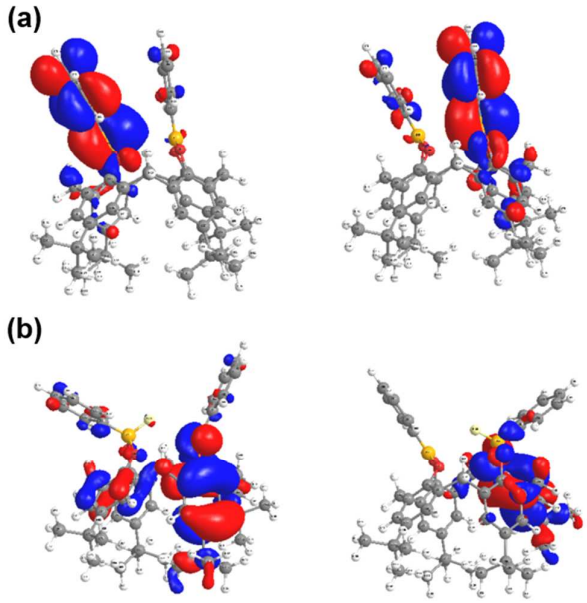

Figure S7. (a) The LUMO and LUMO+1 of 1 in the excited state (b) The HOMO and HOMO-4 of *endo*-1-F in the excited state using PBE1W/6-311G(d)

Figure S7-(a) shows the high electron density in the fluoride-binding region, and thus the change in calculated transitions while binding can be understood as an interaction between **1** and F^-.

S6. Additional TD-DFT calculation using CAM-B3LYP functional

S6.1 Additional TD-DFT calculations using the CAM-B3LYP functional

TD-DFT calculations are also carried out on both **1** and **1-F** using the CAM-B3LYP functional.[5] Table S3 lists the vertical excitation of **1** with corresponding energy, oscillator strength, and major contributing transitions.

Table S3. Vertical excitation of bis(bora)calix[4]arene in the ground state using CAM-B3LYP/6-311G(d)

	Λ_{calc}	Assignment (contribution)	f_{calc}
Band I	251.89 nm	HOMO → LUMO+1 (0.47) HOMO → LUMO (0.16)	0.0004
Band II	247.41 nm	HOMO-1 → LUMO+1 (0.45)	0.0927

S6.2 Additional TD-DFT calculations using the PBE1W functional: Vertical excitation of 1 and *endo*-1-F in the S1 geometry

Table S4. Vertical excitation of 1 and *endo*-1-F in the S1 (excited) state with corresponding energy and oscillator strength using PBE1W/6-311G(d)

(a) bis(bora)calix[4]arene

	Λ_{calc}	Assignment	f_{calc}
Band A	653.10 nm	HOMO → LUMO	0.002
Band B	519.81 nm	HOMO-1 → LUMO	0.001
Band C	383.21 nm	HOMO → LUMO+2	0.009
Band D	378.61 nm	HOMO-1 → LUMO+1	0.032

(b) bis(bora)calix[4]arene with fluoride (the *endo*-binding)

	Λ_{calc}	Assignment	f_{calc}
Band A’	> 700 nm	HOMO → LUMO	0.000
Band B’	590.69 nm	HOMO-1 → LUMO	0.001
Band C’	449.11 nm	HOMO → LUMO+2	0.007
Band D’	368.84 nm	HOMO-1 →LUMO+1	0.001

S7. Reverse S1 → S2 internal conversion calculation: Δ(S1-S2)

S7.1. Schematic description

To determine the origin of fluorescence from the higher excited states, the energy difference of the reverse internal conversion (or the thermal population) from the S1 to the S2 states is needed.[6] Figure S8 shows the scheme of calculating the energy difference, Δ(S1-S2), at the first excited state. This schematic sketch of the potential energy surface (PES) is from Figure 5 in Ref (7).[7]

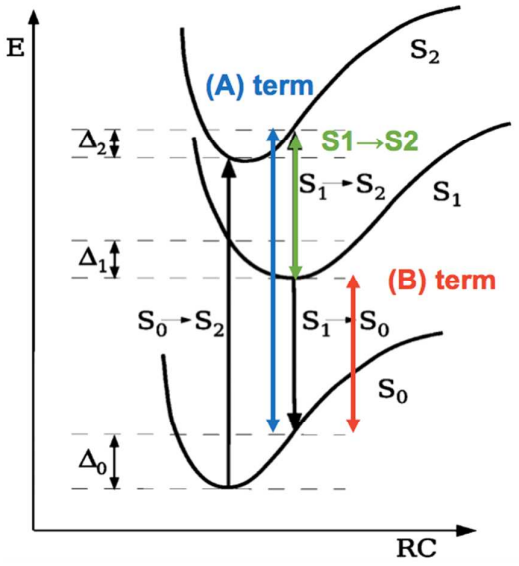

Figure S8. Schematic sketch of PES of the ground state (S0), first (S1) and second (S2) excited states of the selected system along the chosen reaction coordinate[7]

S7.2. Results

To calculate the energy difference Δ(S1-S2), one can decompose the (A) term, which corresponds to the energy difference between the S0 and S2 states of the optimized structure in the S1 state, as:

$$\text{(A) term} = \text{(B) term} + (S1 \rightarrow S2)$$

Here, the (B) term corresponds to the emission energy from the S1 to the S0 states, which can be calculated as the TD-DFT excitation energy from the S0 to the S1 states at the structure optimized in the S1 state. Table S5 shows each term from the equation above and the resultant energy difference, implying that the reverse internal conversion may be very unlikely for **1**.

Table S5. (A) term, (B) term and Δ(S1-S2) values from the simulation using PBE1W/6-311G(d) level of theory

Energy	(A) term	(B) term		Δ(S1-S2)
Explanation	Excitation Energy (S0→S2)	S1 Energy at S1 optimized str.	S0 Energy at S1 optimized str.	*(A) term* – *(B) term*
Value	2.3859 (eV)	-2522.822764 (Hartree)	-2522.892612 (Hartree)	3913.718761 (cm^{-1})
Converted Value	0.087680155 (Hartree)	(B) term = 0.06984794 (Hartree)		0.017832215 (Hartree)

S8. UV-vis calculation of other potential fluoride sensors with group 15 atoms

Figure S9 shows the simulated absorbance spectra of **NN-1**, **PP-1**, **NP-1**, and their *endo*-binding and *exo*-binding complexes. The absorbance $\epsilon(\nu)$ of each spectrum is reproduced by the Harada-Nakanishi equation,[8] which is followed by the equation below:

$$\epsilon(\nu) = \sum_{i=1}^{N} \left(\frac{f_i}{3.483 \times 10^{-5} \sqrt{\pi}\sigma} \times \exp\left(-\left(\frac{\nu - \nu_i}{\sigma}\right)^2\right) \right)$$

where ν is the excitation energy in eV, f_i is the oscillator strength from TD-DFT calculations, and σ is the parameter chosen as 0.330 eV to construct the Gaussian line shapes.

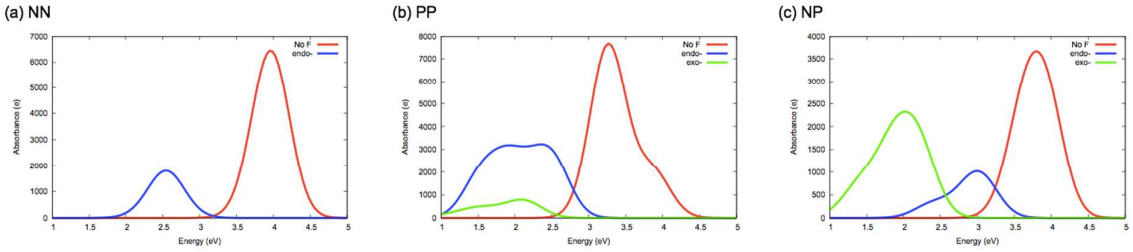

Figure S9. Calculated UV-vis spectrum of X-1, *endo*-X-1-F, and *exo*-X-1-F in the gas phase using PBE1W/6-311G(d) (the shape of spectrum is obtained by employing Gaussian spectrum with half width of 0.330 eV): (a) NN-1 (b) PP-1 (c) NP-1

References

(1) Arimori, S.; Davidson, M. G.; Fyles, T. M.; Hibbert, T. G.; James, T. D.; KociokKo¨hn, G. I. Synthesis and structural characterisation of the first bis(bora)calixarene: a selective, bidentate, fluorescent fluoride sensor. *Chem. Commun.* **2004**, *14*, 1640 – 1641.

(2) Bifulco, G.; Gomez-Paloma, L.; Riccio, R.; Gaeta, C.; Troisi, F.; Neri, P. Quantum mechanical calculations of conformationally relevant ^{1}H and ^{13}C NMR chemical shifts of calixarene systems. *Org. Lett.* **2005**, *7*, 5757–5760.

(3) Bifulco, G.; Riccio, R.; Gaeta, C.; Neri, P. Quantum Mechanical Calculations of Conformationally Relevant ^{1}H and ^{13}C NMR Chemical Shifts of N-, O-, and S-Substituted Calixarene Systems. *Chem. Eur. J.* **2007**, *13*, 7185–7194.

(4) Wang, J.; Bai, F. Q.; Xia, B. H.; Sun, L.; Zhang, H. X. Theoretical Understanding of Ruthenium(II) Based Fluoride Sensor Derived from 4,5-Bis(benzimidazol-2-yl)imidazole (H3ImBzim) and Bipyridine: Electronic Structure and Binding Nature. *J. Phys. Chem. A* **2011**, *10*, 1985-1991.

(5) Yanai, T.; Tew, D. P.; Handy, N. C. A new hybrid exchange–correlation functional using the Coulomb-attenuating method (CAM-B3LYP). *Chem. Phys. Lett.* **2004**, *393,* 51-57.

(6) Itoh, T. Fluorescence and phosphorescence from higher excited states of organic molecules. *Chem. Rev.* **2012**, *112*, 4541-4568.

(7) Dreuw, A. Influence of geometry relaxation on the energies of the S1 and S2 states of violaxanthin, zeaxanthin, and lutein. *J. Phys. Chem. A* **2006**, *110*, 4592-4599.

(8) Harada, N.; Chen, S. M. L.; Nakanishi, K. Quantitative definition of exciton chirality and the distant effect in the exciton chirality method. *J. Am. Chem. Soc*. **1975**, *97,* 5345-5352.